Morphological analysis of Lautaro volcano, Austral Volcanic Zone of the Andes: Insights into the evolution of an active volcano in the Southern Patagonian Ice Field

*José Pablo Sepúlveda[1, 2], Cristián Rodrigo[3]

[1] Facultad de Ingeniería, Universidad Andrés Bello, Quillota 980, Viña del Mar, Chile. jose.sepulveda.b@unab.cl

[2] Millennium Institute on Volcanic Risk Research - Ckelar Volcanoes, Chile

[3] Escuela de Ciencias de la Tierra, Universidad Andrés Bello, Quillota 980, Viña del Mar, Chile. cristian.rodrigo@unab.cl

*Corresponding author: jose.sepulveda.b@unab.cl

ABSTRACT

The Lautaro volcano is the northernmost and highest volcanic center of the Austral Volcanic Zone (AVZ) of the Andes. It is in the northwestern part of the plateau of the Southern Patagonian Ice Field along the northern continuity of the Pío XI chain. The volcano is almost entirely ice-covered, nourishes numerous large outlet glaciers, and has been the object of only very limited field-based geological studies. The volcano is a key location within the Southern Patagonian Ice Field due to its potential influence on the advancement trend cycles of the Pío XI glacier. The present contribution uses the Red Relief Image Map technique to identify volcanic landforms and structures in a glacial context, providing the first quantitative morphological assessment of the Lautaro volcano. The results show plateau-like lava flows at the base of the volcano, possibly concentrically emplaced from a single emission center during the first stages of volcano construction. Subsequent stages comprise two main edifices formed by overlapped lavas and coulées on top, with multiple emission centers aligned along a NE-SW volcanic lineament. The early evolution of the volcano seems to have been influenced by the regional paleotopography. The approximate pre-eruptive surface is relatively flat, with a depression in the northern and eastern sectors of the volcano and a positive relief towards the southern and western parts. Furthermore, a review of the historical activity and tephra records from lakes in Argentina was performed to reassess the eruptive activity of Lautaro. This review reveals a cycle of intermittent historical volcanic activity, with at least three major eruptions during the 1870s and 1880s, and classifies Lautaro as the most active volcanic center in the AVZ, at least since the late 19th century. These antecedents advance our knowledge about the interactions between volcanoes and glaciers in southern Patagonia, providing new perspectives on the evolution of this remote, ice-capped volcano.

Keywords: Red Relief Image Map, Pío XI glacier, Southern Patagonian Ice Field, Lautaro volcano

Análisis morfológico del volcán Lautaro, Zona Volcánica Austral de los Andes: Perspectivas sobre la evolución de un volcán activo en el Campo de Hielo Patagónico Sur. El volcán Lautaro es el centro volcánico más septentrional y de mayor altitud de la Zona Volcánica Austral (ZVA) de los Andes. Se ubica en la parte noroccidental de la meseta del Campo de Hielo Patagónico Sur, a lo largo de la continuidad septentrional de la cadena Pío XI. El volcán se encuentra casi completamente cubierto de hielo, alimenta numerosos glaciares efluentes, y ha sido objeto de escasos y limitados estudios geológicos de campo. El volcán Lautaro representa un caso único dentro del Campo de Hielo Patagónico Sur debido a su posible influencia en los ciclos de avance del glaciar Pío XI. El presente estudio aplica la técnica de Mapa de Relieve en Escala de Rojos (*Red Relief Image Map*) para identificar estructuras y geoformas volcánicas en un contexto glaciar, y proporciona el primer análisis cuantitativo sobre la geomorfología del volcán Lautaro. Se reconocieron flujos de lava con morfologías de tipo meseta en la base del volcán, posiblemente emplazados de manera concéntrica desde un único centro de emisión. Por el contrario, la última etapa comprende dos edificios volcánicos principales formados por superposición de lavas y *coulées* emitidos desde múltiples centros de emisión alineados a lo largo de un lineamiento volcánico de orientación NE-SO. La evolución temprana del volcán habría estado fuertemente influenciada por la paleotopografía regional, con una superficie relativamente plana y deprimida en las porciones norte y este del volcán, y una superficie alzada hacia los sectores sur y oeste. Se incluye, también, una revisión detallada de la actividad histórica y de los registros lacustres de tefra en Argentina con el objetivo de actualizar la actividad eruptiva de este volcán. Los registros históricos revelan un ciclo de actividad volcánica intermitente con al menos tres erupciones importantes durante las décadas de 1870 y 1880, por lo que el Lautaro correspondería el centro volcánico más activo en la ZVA, al menos desde finales del siglo XIX. Estos antecedentes amplían el conocimiento acerca de las interacciones entre volcanes y glaciares en la zona sur de la Patagonia, y proporcionan nuevas perspectivas sobre la evolución de este remoto volcán.

Palabras clave: Glaciar Pío XI, Mapa de Relieve en Escala de Rojos, Campo de Hielo Patagónico Sur, Volcán Lautaro

1. Introduction

The Austral Volcanic Zone of the Andes (AVZ; Fig. 1A) hosts several remote and poorly studied volcanic centers, many of which are located within the Southern Patagonian Ice Field (SPI; Stern and Kilian, 1996) (Fig. 1B). Geological and tephrochronological antecedents suggest that some AVZ volcanoes have produced large explosive eruptions during the Holocene (Motoki et al., 2006; Stern, 2007; Fontijn et al., 2010; Wastegård et al., 2013; Smith et al., 2019), and highlight the need to constrain their eruptive history, morphological evolution, and potential geohazards. The identification of volcanic landforms in glacial, remote environments is, however, quite challenging: the presence of snow and ice sheets masks the contact between volcanic structures and the surrounding area, while deposits derived from glacial erosion, such as moraines, till, or outwash deposits, result in a general smoothing of the morphological differences. Lautaro volcano, situated near the north-center of the SPI at ~49° S and ~73.5° W (Fig. 1B), exemplifies such challenges well. The volcano is almost entirely ice-covered (Fig. 1C), and any field-based geological study is limited by harsh climate conditions, logistical constraints, and hazardous terrain. Despite reports of historical volcanic activity (e.g., Motoki et al., 2006; Martinic, 2008; Petit-Breuilh, 2022), available data are scarce, uncertain, and lack systematic analyses. Lautaro also represents an unusual case within the SPI due to its potential influence on the almost permanent state of advance of the Pío XI glacier (Fig. 1C), the largest tidewater glacier in the SPI (Warren et al. 1997; Rivera, 2018). Previous studies have speculated that geothermal or volcanic activity may partially control the glacier's advance and retreat cycles (Wilson et al., 2016; Rivera, 2018).

The Red Relief Image Maps (RRIMs; Chiba et al., 2008) are Digital Elevation Model (DEM) derived images, which allow the identification of volcanic landforms and structures based on the terrain slope and openness (Chiba et al., 2008; Karátson et al., 2016; Favalli and Fornaciai, 2017; Ulusoy et al., 2021; Sepúlveda et al., 2026). Previous studies have shown the applicability of RRIMs to identify and map volcanic structures in desert contexts (Ulusoy et al., 2021; Sepúlveda et al., 2025) and in pervasive vegetated areas (Benvenuti et al., 2014; Sepúlveda et al., 2026), yet its applicability in glaciated environments has not been introduced to date. This study therefore provides the first quantitative morphological assessment and geomorphological map of Lautaro volcano by applying the RRIM technique, to investigate the effect of the pre-eruptive topography on the volcano's evolution. To complement these findings, a review of the historical activity of Lautaro, which includes tephra records from lakes in Argentina, is presented to reassess its eruptive activity

2. Geological setting of the AVZ

The AVZ is the southernmost volcanically active segment of the Andes (Fig. 1A), occurring between latitudes 49° S and 55° S (Stern et al., 1976, 2007; Stern, 2004). It results from the subduction of the oceanic lithosphere of the Antarctic plate below the continental lithosphere of the South American plate at a velocity of 2-3 cm/yr (Stern, 2007). The northern boundary of the AVZ corresponds to the eastern projection of the Chile Ridge, which separates the Nazca plate from the Antarctic plate (Stern, 2004; Stern et al., 2007). At the Chile Triple Junction (~46° S), which is where the Chile Ridge meets the South American continent, young (<6 Ma) oceanic lithosphere is being subducted, producing the Patagonian gap, a ~350 km-long zone without active volcanism at the active margin (Kilian, 1990; Stern et al., 2007). The age of the Antarctic plate at the trench changes from 12 Ma in the northern sector of the AVZ to 24 Ma in the south, without a Benioff zone of seismic activity (Ramos et al., 1982; Stern and Kilian, 1996; Stern, 2004; Stern et al., 2007). The crustal thickness below the AVZ is <35 km, with a pre-Andean basement comprising late Paleozoic to early Mesozoic sedimentary and metamorphic rocks (Stern, 2004).

The AVZ comprises four stratovolcanoes and a dome complex (Puig et al., 1984; Stern, 2004) (Fig. 1B). The northernmost Lautaro and Aguilera volcanoes occur within the SPI and have similar chemical compositions (Stern et al., 1984; Stern and Kilian, 1996; Stern, 2004), while the Reclus, Monte Burney, and Cook Island volcanoes form the southern portion of the AVZ.

About 45 km SE of Lautaro, a topographic high named Viedma was considered an active volcano for decades due to its air-view morphology (Lliboutry, 1956, 1998; Kilian, 1990; González-Ferrán, 1995; Kobayashi et al., 2010) and loose tephra clasts sampled over the SPI in its surroundings (Kilian, 1990). However, field surveys later determined a non-volcanic nature for Viedma, with outcrops composed of very-low grade metamorphic rocks (Shipton, 1963; Blampied et al., 2012; Suárez et al., 2019).

2.1 Southern Patagonian Ice Field

The SPI stretches for ~350 km, covering ~13,000 km^2 between latitudes 48°20' S and 51°30' S (Millan et al., 2019; Bravo et al., 2021). The ice surface has a mean elevation of 1,500 to 2,000 m a.s.l. and is punctuated by numerous nunataks, with Lautaro volcano forming the highest peak in the region (Warren and Sugden, 1993). In the SPI, most of the ice flow distributions are strongly controlled by topography (Millan et al., 2019). By combining airborne gravity with radar data, Millan et al. (2019) mapped the bedrock elevation and the ice thickness in the SPI, identifying deep glacial valleys with thicknesses exceeding 1,400 m and sectors with bedrock below sea level. Southwest of Lautaro, the Pío XI glacier forms the largest glacial basin of the SPI. Here, the glacier presents a thickness >1,300 m with a relatively flat bedrock and sectors 200 m below sea level (Millan et al., 2019). The glacier terminates at two fronts: the northern front calves into Greve lake, and the southern front reaches the ocean at Eyre fjord. Unlike other glaciers in the SPI, Pío XI has been advancing and thickening over the last several decades (Sakakibara and Sugiyama, 2014; Rivera, 2018; Minowa et al., 2019).

2.2 Geology of the Lautaro volcano

The Lautaro volcano (3,607 m a.s.l.) is the northernmost and highest volcanic center of the AVZ. It is located along the northern continuity of the Pío XI chain, a ~20 km long NE-SW chain comprised of metamorphic rocks, and feeds numerous large outlet glaciers (Figs. 1C and 2), most of which terminate at calving cliffs in the Chilean fjords or in the big Argentine lakes. The bedrock geology is poorly constrained due to the presence of the SPI, with the basement only well-exposed along the lateral walls of the fjords in the western flank of the volcano. The bedrock comprises low-grade pelitic metamorphic rocks intruded by hornblende-biotite granites (Motoki et al., 2006). The geology and structures of the volcano are restricted to general sketches based on aerial photographs (González-Ferrán, 1995; Orihashi et al., 2004). Petrochemical data are scarce and poorly defined; typically, major elements have been defined and contrasts with other centers from the AVZ provided (Futa and Stern, 1988; Stern and Kilian, 1996; Stern et al., 2007). Samples from the volcano are restricted to reworked material obtained from terminal moraines from the HPS9 glacier, ~17 km west of the volcano (Orihashi et al., 2004; Motoki et al., 2003, 2006) (Fig. 1C), and from tephra layers sampled from lakes in Argentina and loose ash/pumice collected from Viedma and O'Higgins glaciers (del Valle et al., 1995; Motoki et al., 2006; Villegas et al., 2009; Kastner et al., 2010; Wastegård et al., 2013; Mayr et al., 2019; Smith et al., 2019; Charqueño-Celis et al., 2024).

Due to its remoteness and inaccessibility, radiometric data from Lautaro are restricted to nine whole-rock, unspiked K-Ar ages from reworked material incorporated in a terminal moraine from the HPS9 glacier (Orihashi et al., 2004). Three of these samples presented large analytical errors and did not yield reliable ages, whereas the remaining six ages were grouped into two clusters: 168-161 ka and 114-97 ka. That is, activity at Lautaro would have begun at around 170 ka, at least (Orihashi et al., 2004).

In terms of explosive activity, Smith et al. (2019) identified one tephra layer around Laguna Potrok Aike, 400 km to the SE, likely sourced from the Lautaro volcano. The geochemistry of this material was provided by Mayr et al. (2019), and an age of ca. 43.4 cal ka BP estimated by Gebhardt and Ohlendorf (2019). In this sector, two other tephra layers present geochemical affinities to Lautaro but are petrographically distinct, so no correlations were suggested (Smith et al., 2019). Closer to the volcano, at around 50 km east, four historical (>1850 AD) tephra layers from the Laguna Gemelas Este and Laguna Verde areas in Argentina were tentatively assigned to Lautaro by Mayr et al. (2019) based on ^{137}Cs and ^{210}Pb dating. Finally, tephra layers reported in the Laguna del Desierto area, ~45 km E of Lautaro, were assigned to the 1959-60 eruptive cycle by Kastner et al. (2010).

3. Methodology

3.1 Red Relief Image Map

The Red Relief Image Map (RRIM; Chiba et al., 2008) is a non-directional and multi-layered single image that improves the topography visualization by combining the slope and the topographic openness. Here, the RRIM was analyzed based on an Advanced Land Observing Satellite Phased Array L-band Synthetic Aperture Radar (ALOS PALSAR) DEM of 12.5 m pixel resolution from the Alaska Satellite Facility's Radiometric Terrain Correction Project.

Topographic openness is an angular measure of the relation between surface relief and horizontal distance calculated from the average of multiple zenith or nadir angles for eight compass directions (Yokoyama et al., 2002). A positive openness (ϕ_R) expresses openness above the surface, highlighting convex, positive relief landforms (e.g., emission centers, crests, ridges), while a negative openness (Ψ_R) describes this attribute below the surface, highlighting concave, depressed landforms (e.g., valleys, gorges, craters). Topographic openness is inherently scale-dependent as it is a function of the shape and radius of the selected neighborhoods (Yokoyama et al., 2002; Favalli and Fornaciai, 2017; Sepúlveda et al., 2026). The differential openness (ϕ) is a function of ϕ_R and Ψ_R:

$$\phi = \frac{\phi_R - \Psi_R}{2} \quad (1)$$

The ϕ parameter is positive when the surface, at the selected search radius (R), is upwardly convex and negative when the surface is upwardly concave (Chiba et al., 2008; Favalli and Fornaciai, 2017). For the Lautaro volcano, a 1,000 m radius search was tested to identify major landscape units while avoiding background noise (Sepúlveda et al., 2026).

Slope is visualized in a red shading by using the Hue-Saturation-Value color fusion technique (Favalli and Fornaciai, 2017; Hema and Kannan, 2019), rendered with a continuous color ramp and providing a smooth visual transition across the slope range. Similarly, the differential openness is displayed with a greyscale ramp, so when combined with the slope it covers the black-red-white color range. Morphological characteristics were highlighted in ϕ by applying a mean ± standard deviation (σ) filter to enhance image contrast. Following Favalli and Fornaciai (2017), a 2.5σ stretching equalization filter was applied to ϕ since it maintains a suitable compromise between the image display and the shape of the histogram.

The RRIM results are shown in figure 2. Top ridges are displayed as white, bottom valleys as black, steep slopes as bright red, and flat surfaces as gray (Chiba et al., 2008; Ulusoy et al., 2021; Sepúlveda et al., 2025, 2026). Similarly, emission centers are enhanced as rounded to convex reliefs, typically surrounded by flat or incised areas, or flat-topped (<5°) areas flanked by steep slopes identifiable as punctual to rounded bright-white zones (Sepúlveda et al., 2025, 2026). The volcano boundary was defined assuming that volcanic edifices are bounded by concave breaks in slope (Euillades et al., 2013; van Wees et al., 2024; Sepúlveda et al., 2025). For this, the volcano boundary was manually delineated based on the RRIM, with a slope threshold of 3° applied as a maximum guiding criterion (van Wees et al., 2024). This threshold provides an approximation of the transition from volcanic deposits to the surrounding ring plain.

3.2 Pre-eruptive surface modeling

The pre-volcano topography was modeled from a series of points in a grid containing the volcano. Once the boundary of the volcano was defined, a 5 m square mesh was generated containing the volcano and comprising 15,499,088 points. The ALOS PALSAR DEM was resampled to 5 m pixel/resolution, assigning UTM coordinates and height values to each point of the mesh and removing from the mesh all points located within the volcano boundary (Kereszturi et al., 2016; Sepúlveda et al., 2023). Later, the height data were interpolated to a first-order surface (i.e., planar) by using a Triangular Irregular Network (TIN) and applying the Delaunay criteria to maximize each triangle's minimum angle (Sepúlveda et al., 2023). Due to the continuous surface of the SPI, the surrounding topography was assumed to represent the buried pre-eruption landscape, with major topographic breaks only occurring at the southern and western boundaries of the volcano. Finally, the pre-Lautaro topography was generated by rasterizing the TIN surface. A thickness map for the volcano was generated by subtracting the height data of the modeled pre-eruptive surface from the current topography on a cell-by-cell basis, with the eruptive volume calculated as the 3D space enclosed by the pre-eruptive surface and the current topography (Sepúlveda et al., 2023, 2025). In case of returned negative thicknesses due to underestimations in the true pre-eruption topography, they were reassigned to zero.

4. Results

4.1 Volcanic edifice delimitation

The RRIM shows clear morphological and textural differences between volcanic terrains and the surrounding SPI and the Pío XI chain (Fig. 2). Lautaro has steep edges in its upper part, shown in the RRIM as bright red, while the upper surfaces, flow advancement lobes and central channels of lava flows are displayed as continuous white surfaces. At its base, the volcano presents rough, heterogeneously colored (black to white) surfaces, probably related to highly eroded lavas or moraines/glacial deposits, and diffuse white zones at the fronts of possible lava flows. Conversely, the surrounding SPI has a smooth surface without important relief variations, shown in the RRIM as a continuous and homogeneous gray surface. These morphologies also strongly contrast with the Pío XI chain south of Lautaro. In this sector, the RRIM highlights the chain as a positive relief with continuous and white convex linear crests in its axial part. These crests typically present a polygonal shape and are flanked by red, steep slopes and a grey, smooth and homogeneous relief downslope. Contrary to volcanic terrains, the Pío XI chain and its surroundings do not present features indicative of lava lobes or other volcanic landforms.

4.2 The paleotopography of the Lautaro volcano

The modeling of the pre-eruptive surface indicates a strong control of the paleotopography on the emplacement of Lautaro's basal products. The northern and eastern sectors of the edifice were underlain by a relatively flat, depressed surface, whereas the southern and western sectors rested on a topographically higher ground (Figs. 3 and 4A). The transition between the northeastern planar surface and the southwestern upraised structure seems to occur around the area of the current summit of Lautaro (Figs. 3 and 4B). This upraised structure could either be the northern projection of the Pío XI chain or part of the metamorphic basement that outcrops west of the volcano (Figs. 3 and 4). This paleotopography is consistent with the irregular and unequal altimetric distribution of the Lautaro lavas (Fig. 3). In the northern half of the volcano, lava flows typically descend to altitudes between 1,400 and 1,500 m a.s.l., in correspondence with the topography of the SPI. Conversely, in the southern half of the volcano, the contacts with the substrate typically occur at altitudes above 1,700 m a.s.l., with lavas even emplaced above the Pío XI chain over 2,000 m a.s.l. This asymmetry in the Lautaro lavas also agrees with the gentler slopes towards the northern flank of the volcano and steep-walled lava flows to the south (Figs. 3 and 4B).

4.3 Emission centers of the Lautaro volcano

In the Lautaro volcano, several emission centers were identified through the RRIM, with two main edifices (northern and southern) separated by a high pass (Figs. 2 to 4). The southern edifice comprises thick lavas emitted towards the eastern and southern flanks, whereas the northern edifice is the current, active summit of Lautaro, formed by overlapped lavas emplaced concentrically from the emission center (Fig 5). Fumarolic activity is present around Lautaro's active summit (Motoki et al., 2006).

From the northern, active edifice to the northeast, there are at least five NE-SW oriented emission centers (Fig. 2). Two kilometers from the main edifice there is a pyramid-shaped center (Mimosa) from which a lava flow was emitted to the east to a maximum distance of 5.8 km (Fig. 2). Fumarolic activity was reported at Mimosa in 1973 by a group of mountaineers (Lliboutry, 1998). Based on the lava morphologies and emplacement directions interpreted from the RRIM, Mimosa would be older than the northern edifice, as a lava flow from the latter seems to have been diverted to the northwest by the former (Fig. 5A).

From Mimosa, two kilometers to the northeast, lies Pangrec, a small pyramidal center with short, concentric lobes with steep slopes (Figs. 2 and 5B). From Pangrec to the northeast, an ~850 m long coulée is observed, whereas to the north there are remnants of a small and older caldera rim (Gorra Blanca; Lliboutry, 1998) (Fig. 5B). This caldera is open to the east and elliptical in plain view, with a NE-SW elongation and a maximum radius of ~2 km. It has steeper outer flanks, with thicknesses of up to 200 m showing eroded spine-like structures. As it is cut by the Pangrec lavas, Gorra Blanca would be older (Fig. 5B).

Finally, a small and isolated parasitic center ~6 km WNW from the northern edifice is observed (Figs. 2 and 5C). This lateral center occurs north of the HPS9 glacier and corresponds to an ~250 m thick lava-dome that grew radially around the vent, from which an ~80 m thick and ~1,9 km long lava flow was emitted to the northwest (Fig. 5C).

4.4 RRIM-identified lava flow units of the Lautaro volcano

The remote reconnaissance of the Lautaro volcano allows the identification of different lava flows based on their topographic positions, structures, and surficial textures. By analyzing the RRIM, these lava flows can be grouped into four main morphological units (Fig. 6).

The topographically lower identified unit (Lautaro I) corresponds to highly eroded lava flows at the base of the volcano that mainly outcrop towards the eastern and northern flanks. The lavas of this unit show smooth to planar surfaces without preserved structures, being only recognized based on convexities of the terrain and slope breaks (Figs. 2 and 6). They are covered by the glacial ice sheet and are apparently eroded and covered by glacial deposits.

Two lava flows present maximum runouts of ~5 km from the current summit and maximum thicknesses of ~100 m.

The Lautaro II unit lies topographically above the Lautaro I lavas. This unit comprises overlapped lava flows emplaced radially around the two main edifices. These lavas are highly eroded by glacial activity, typically presenting carved U-shaped incisions (Figs. 2, 4, and 6). In the northern flank of Lautaro, they exhibit plateau-like morphologies with well-preserved, smoothed flow fronts, forming a stepped relief consisting of a series of overlapping plains separated by breaks in the slope. On the other hand, in the southern flank they present steep slopes and rough surfaces. Although there is no clear topographical relationship between the Lautaro II lavas and the small lateral center to the northwest (Lautaro III), a younger age for the lateral center is suggested based on its relatively better-preserved morphology.

The Lautaro IV unit covers Lautaro II and the caldera rim of Gorra Blanca. This unit consists of lava flows and coulées emplaced from multiple peaks (Figs. 2 and 6). To the north, this unit comprises the centers formed along the NE-SW lineament, from which overlapping, steep, and short runout lavas were emitted. Arcuate ridges displayed concentrically to their respective emission points are also observed (Fig. 5A). To the south, the lavas were possibly emitted from a unique emission point (Fig. 6). They are long and narrow and present steep edges, lateral lobes, and subrounded toes. In their medial portions they are flat-topped and show well-preserved transverse to flow arcuate ridges in their proximal and distal parts, in concordance with the steeper slopes. From this unique southern vent, the lavas flowed into three main branches (Fig. 6): (1) to the east, where they feature overlapping toes in their fronts, (2) a short and unique ~2.5 km-long flow to the southeast, and (3) an ~11 km-long lava towards the south, which diverted into two main lobes at ~4 km from the vent.

4.5 RRIM-identified glacial landforms in the Lautaro volcano area

In the Lautaro volcano area, a number of erosive and accumulative landforms of glacial origin can be identified from the RRIM. In this map, escarpments are highlighted as continuous, linear to curved red structures related to steep-side zones (>40°), typically within the edges of topographically higher lava flows (Figs. 2 and 6). Glacial cirques are bowl-shaped, amphitheater-like, and steep-walled depressions that occur in the upper flanks of the volcano. In the RRIM, they are visualized as black-bottomed valleys flanked by red zones in the slopes facing the volcano (Fig. 2). They form U-shaped and rough-bottomed valleys downslope, probably infilled by moraines and rockfall talus slope deposits. U-shaped valleys, in general, occur along all the volcano boundaries. They are flanked by escarpments showing open and semi-circular shapes, and vary from small, typically 400 m wide, deep depressions with nearly vertical slopes at their uppermost sectors to 1,700 m wide, smooth flat-bottomed depressions (Fig. 6).

4.6 Records of historical activity from the Lautaro volcano

The Lautaro volcano has been mentioned with different names in historical documents and by the local population (e.g., Chaltén, Cerro Pirámide, Volcán de los Gigantes, Humboldt, Mano del Diablo). In Argentina, the early explorers of Patagonia were told by natives that an active volcano was present to the west, somewhere within the ice field (Moreno, 1879; Lista, 1880; Quensel, 1911; de Agostini, 1945; Lliboutry, 1957; Martinic, 2008). This then-unknown active center was for decades misidentified as the Fitz Roy, a peak ~40 km SE of Lautaro, until its non-volcanic nature was established, with Carlos Moyano proposing in 1884 the location of this active volcano someplace northwest of Fitz Roy (Moyano, 1931; de Agostini, 1945; Martinic, 2008).

Due to its remoteness, reports typically comprise memoirs and tales from explorers, settlers from Argentina (that is, more than 100 km to the east), and logbooks from voyages of the British and German Navy. Records of historical volcanic activity from Lautaro are summarized in Table 1. The large number of eruption reports during the 1870s and 1880s may reflect a cycle of intermittent volcanic activity. This cycle included ash emissions, minor eruptive columns, and incandescence, with major events in 1879, 1883, and 1884 (Kólliker et al. 1917; Martinic, 2008; Greenwood, 2015). However, despite all this evidence, Lautaro was only officially recognized as an active volcano in 1933 after the expedition led by Federico Reichert, who reached its base and observed gas and ash emissions. This discovery was unfortunately not widely disseminated, so the mystery of an active volcano somewhere in the SPI remained for a couple of decades (von Rentzell, 1933, 1934a, b, c; Reichert, 1947).

On 28th December 1959, Alfonso Cuadrado Merino, a pilot from the *Linea Aérea Nacional,* observed and photographed an eruption column from Lautaro (Martinic, 1960a, b, 1988; González-Ferrán, 1995). Some weeks later, the expedition led by Eric Shipton arrived at the base of Lautaro on 19th January 1960, locating it cartographically (Shipton, 1960, 1963).

Eruptions during the second half of the 20th century were far less recurrent, comprising activity reported by farmers in Argentina and ephemeral tephra blankets remotely identified over the SPI (Kilian, 1990; Lliboutry, 1998). Petit-Breuilh (2022) mentions two eruptions in 1995 and 1998; however, we did not find any report or bibliographic reference regarding an eruption during the 1990s for this volcano. Finally, Motoki et al. (2006) sampled undated tephra fragments from the terminal part of the O'Higgins glacier, recognizing at least three fallout layers that may correspond to the latest eruptions.

5. Discussions

5.1 Geomorphology of the Lautaro volcano

The Lautaro volcano forms an ~N-S elongated relief along the northern continuation of the Pío XI chain. The modeled pre-eruptive surface indicates a depressed and flattened area towards the northeastern sector and a morphological elevation to the southwest, the latter in correspondence to the metamorphic basement highs (Figs. 3 and 4A). The volcano consists of several overlapped shield-like lava flows at the base (Lautaro I and Lautaro II units; Fig. 6), and viscous, superimposed lava flows and coulées emplaced from multiple lateral vents that form the volcano's upper part (Lautaro III and Lautaro IV units; Fig. 6). The morphology of the uppermost part of the volcano had already been recognized by Orihashi et al. (2004), who described a dome or coulée complex rather than a compound volcano. By calculating the mass in excess between the current and pre-eruptive surfaces within the volcano boundary, it is found that Lautaro has a volume of 52 km^3. The isopach map of Lautaro upon which this calculation was done is shown in figure 7.

Flank vents reflect magma ascent paths and can give insights into the underlying magmatic system and growth processes (Acocella and Neri, 2009; Yokoyama, 2015). The concentric distribution from the current summit of the oldest identified lavas may suggest a volcano-related concentric stress field during the first stages of volcano construction (Nakamura, 1977). On the other hand, the alignment of emission centers during the last stage (Lautaro IV) strongly suggests the influence of the regional stress field in controlling dyke propagation, similar to other volcanic centers such as Etna (Italy), Ollagüe (Chile) or Miyake (Japan) (Nakamura, 1977; Vezzoli et al., 2008; Acocella and Neri, 2009; Yokoyama, 2015).

Initial lavas may have flowed towards the topographically lower eastern and northern flanks, and only after they infilled the depressed surface they started flowing concentrically, similar to what was observed in Monte Amiata (Italy), for example (Principe et al., 2017). The topographic effect of the Pío XI chain on the evolution of Lautaro is reflected in: (1) a major proportion of Lautaro I lavas towards the northern and eastern flanks of the volcano (Fig. 6); (2) Lautaro II lavas with plateau-like morphologies (typically related to lower slopes; Principe et al., 2017; Sepúlveda et al., 2023) in the northern sector and steep, rough surfaces toward the southern flank (Fig. 2); (3) the presence of negative values from the modeled thickness for the volcano in its southwestern and southeastern flanks (Fig. 7), attributable to incised or steep areas without deposition, in concordance with the bedrock elevations determined by Millan et al. (2019), with differences in altitude of up to 1,400 m; (4) one lava flow from Lautaro IV diverted into two branches in the southern flank due to a barrier effect of the Pío XI chain (Figs 2 and 6): the western lobe rapidly halted due to channeled effects on high slopes, and the eastern lobe accelerating because of the barrier effect (e.g., Dietterich et al., 2015); and (5) thicker-than-expected lava flows in the Mimosa and Pangrec areas due to the depressed northern flank (Figs. 3 and 7).

By considering the total calculated volume (52 km^3) and the oldest reported age (ca. 170 ka; Orihashi et al., 2004), we calculate a time averaged volumetric eruption rate of 0.30 km^3/kyr for the Lautaro volcano. This rate represents a maximum, as the Orihashi et al. (2004) ages lack stratigraphic control, with the possibility of older ages emerging as more geological information about the volcano becomes available. In terms of regional comparisons, there is unfortunately no data to contrast with other AVZ centers, although Lautaro's maximum growth rate is similar to those obtained for other centers in the more active SVZ, such as Calbuco (0.35 km^3/kyr; Sellés and Moreno, 2011) or Osorno (0.88 km^3/kyr; Moreno et al., 2010). Further studies are necessary to reveal Lautaro's geological and geochemical evolution.

5.2 Limitations and DEM-resolution effect

RRIMs are inherently a function of the spatial resolution of the input elevation data, a dependency that can have significant implications for delineating specific landforms (Mashimbye et al., 2014). Previous studies have demonstrated that a precise and consistent delineation of the volcanic landforms holds greater significance than the specific DEM type (Kervyn et al., 2006; Van Wees et al., 2024). Similarly, Sepúlveda et al. (2026) showed a good consistency for the terrain surface representation between RRIMs derived from a 1 m pixel resolution Light Detection and Ranging (LiDAR) and those from a 10 m pixel resolution TINITALY DEM in a pervasively vegetated volcanic zone. Therefore, although devoid of a high-resolution DEM for the study area, the 12.5 ALOS PALSAR DEM can be considered to represent the terrain realistically.

The scale of the reliefs identified through the RRIMs are directly related to the selected search radius (Yokoyama et al., 2002; Chiba et al., 2008; Favalli and Fornaciai, 2017; Sepúlveda et al., 2026). A recent study showed that a 100 m search radius realistically represents the ground surface for mapping purposes (Sepúlveda et al., 2026). However, in our case study the surface is best represented by a larger search radius (1,000 m), with lower values increasing the background noise due to local roughness and a major effect of smaller-scale artifacts (Fig. 8). These artifacts are DEMs imperfections resulting in erroneous features that do not exist in the actual terrain, such as spikes, sinkholes, steps, pixel defects, unfilled voids, and line errors, due to incoherent altitude values after DEM acquisition and processing (Hirt, 2018). Here, local scale artifacts as small voids may be enhanced in ice-covered surfaces due to specular effects (Parrot and Ramírez Nuñez, 2015). Finally, although the RRIMs can be used to identify and map several landforms, in volcanic terrains they are uniquely able to recognize lava flows.

5.3 The Viedma nunatak and its implications to historic eruptions of Lautaro volcano

Since the 1960s, field-based studies (Shipton, 1963; Blampied et al., 2012; Suárez et al., 2019) have evidenced the non-volcanic nature of the nunatak Viedma, being removed from the Smithsonian's Global Volcanism Program database in 2019. In the decades in between, however, some still considered it as a volcanic center (Stern and Kilian, 1996; Stern et al., 2007; Kobayashi et al., 2010), even assigning to it an undistinguished geochemical signature with Lautaro volcano (Smith et al., 2019). The non-volcanic nature of Viedma opens two discussions: (1) the tephra analyses formerly attributed to Viedma (Kilian, 1990; Stern and Kilian, 1998; Stern, 2007; Mayr et al., 2019) would rather be from Lautaro, and (2) the records of possible historical activity assigned to Viedma would correspond to Lautaro instead. These records include ash bands identified from aerial photographs in February 1952 (Lliboutry, 1956), and remobilized tephra fragments from an eruption that would have occurred between September and November 1988 (Kilian, 1990). This eruption is recorded, and dated, in the Laguna Gemelas Este in Argentina (Mayr et al., 2019), and may be the last confirmed eruption of the Lautaro volcano.

6 Conclusions

The application of RRIMs proved to be an effective tool for characterizing the geomorphology of volcanic terrains in glaciated and remote environments, allowing the identification of volcanic structures otherwise obscured by the ice cover. At the Lautaro volcano, the RRIM analysis shows overlapped lava flows and coulées, and structures such as a caldera rim, a volcanic lineament, and glacial escarpments. The RRIM reveals two main volcanic edifices: one to the north, comprised by overlapped short runout lavas, and the other to the south, formed by long runout lava flows. In the northern sector, multiple emission centers were emplaced along a NE-SW lineament. Based on morphological features and surface texture of the lava flows, we present the first geomorphological map of Lautaro volcano. This map identifies the remnants of a small caldera rim and four main stages of volcano construction. The modeled pre-eruptive surface, together with the emplacement directions, slopes, and surficial structures of lava flows, indicate that the volcano's morphology was strongly influenced by the regional topography. On the other hand, historical records indicate that Lautaro has been the most active volcanic center in the AVZ since the late 19th century, underscoring the need for further investigation and monitoring of this ice-covered volcano. This study offers new insights into Lautaro's evolution and contributes to a broader understanding of volcano-glacier interactions in southern Patagonia.

Acknowledgements

This research was supported by the National Agency for Research and Development (ANID-Chile), through FONDECYT Regular Project No. 1250354 awarded to C. Rodrigo. Comments. Editorial work from D. Bertin and revisions from A. Graettinger, C. Gómez, and R. van Wees are greatly appreciated.

REFERENCES

Acocella, V.; Neri, M. 2009. Dike propagation in volcanic edifices: overview and possible developments. Tectonophysics 471 (1–2): 67-77.

Benvenuti, M.; Cioni, R.; Conticelli, S.; Francalanci, L.; Lavorini, G.; Marroni, M.; Pandolfi, L. 2024. Note Illustrative della Carta Geologica d'Italia alla scala 1:50.000, F. 320 Castel del Piano. ISPRA - Servizio Geologico d'Italia 320: 399 p. Roma. https://doi.org/10.15161/oar.it/211736

Blampied, J.; Barberon, V.; Ghiglione, M.; Leal, P.R.; Ramos, V. 2012. Disambiguation of the Nunatak Viedma: a basement block previously confused as a volcanic center. In: XIII Congreso Geológico Chileno, Universidad Católica del Norte, Antofagasta, Chile.

Brassey, T. 1880. A voyage in the Sunbeam. Longmans Green & Co. London.

Bravo, C.; Bozkurt, D.; Ross, A.N.; Quincey, D.J. 2021. Projected increases in surface melt and ice loss for the Northern and Southern Patagonian Icefields. Scientific Reports 11 16847 https://doi.org/10.1038/s41598-021-95725-w

Burmeister, C.V. 1891. Breves datos sobre una escursion a la Patagonia. Rev Museo de la Plata 2: 381–394

Casertano, L. 1962. La actividad volcánica en Chile durante 1961. Bol. Univ. De Chile 30 (40). Santiago.

Charqueño-Celis, F.; Dubois, N.; Zolitschka, B.; Pérez, L.; Mayr, C.; Massaferro, J. 2024. Climate and environmental history of Laguna Polo, Santa Cruz, Southern Patagonia (49°S) since 1300 CE. J Paleolimnol 72:163–178. https://doi.org/10.1007/s10933-024-00328-w

Chiba, T.; Kaneta, S.I.; Suzuki, Y. 2008. Red relief image map: new visualization method for three dimensional data. Int. Arch. Photogramm. Remote. Sens. Spat. Inf. Sci. 37: 1071-1076.

de Agostini, A.M. 1945. Andes Patagónicos. Viajes de Exploración a la Cordillera Patagónica Austral. Tomo I. Centro de Investigaciones Diego Barros Arana de la Dirección de Bibliotecas, Archivos y Museos: 478 p. Santiago. ISBN 978-956-8306-08-3

del Carlo, P.; Di Roberto, A.; D'Orazio, M.; Petrelli, M.; Angioletti, A.; Zanchetta, G.; Maggi, V.; Daga, R.; Nazzari, M.; Rocchi, S. 2018. Late Glacial-Holocene tephra from southern Patagonia and Tierra del Fuego (Argentina, Chile): a complete textural and geochemical fingerprinting for distal correlations in the Southern Hemisphere. Quat. Sci. Rev. 195: 153-170.

Del Valle, R.A.; Skvarca, P.; Mancini, V.M.; Lusky, J. 1995. A preliminary study of sediment cores from Lago Argentino and fluctuations of Moreno Glacier, Argentina. Bulletin of Glacier Research 13: 121-126.

Dietterich, H.; Cashman, K.V.; Rust, A.; Lev, E. 2015. Diverting lava flows in the lab. Nature Geoscience 8: 494–496

Euillades, L.; Grosse, P.; Euillades, P. 2013. NETVOLC: An algorithm for automatic delimitation of volcano edifice boundaries using DEMs. Computers & Geosciences 56: 151-160

Favalli, M.; Fornaciai, A., 2017. Visualization and comparison of DEM-derived parameters. Application to volcanic areas. Geomorphology 290: 69-84

Fontijn, K.; Lachowycz, S.M.; Rawson, H.; Pyle, D.M.; Mather, T.A.; Naranjo, J.A.; Moreno-Roa, H. 2014. Late Quaternary tephrostratigraphy of southern Chile and Argentina. Quat. Sci. Rev. 89: 70-84.

Futa, K.; Stern, C.R. 1988. Sr and Nd isotopic and trace element compositions of Quaternary volcanic centers of the southern Andes. Earth Planet Sci Lett. 88: 253-262.

Gebhardt, C.; Ohlendorf, C. 2019. Revised Age Model for Composite Core 5022-2CP, Laguna Potrok Aike, Patagonia. PANGAEA. https://doi.pangaea.de/10.1594/PANGAEA.901831.

Göll, F. 1904. Die Erdbeben Chiles: Ein Vezeichnis. Kessinger Publishing: 148p.

González-Ferrán, O. 1995. Volcanes de Chile. Instituto Geográfico Militar: 640 p. Santiago.

Greenwood, W.H. 2015. Patagonia Bravía. Naturaleza, vidas y aventuras. Memorias originales del baqueano William H. Greenwood. LibroVerde: 341 p. Santiago.

Hema, D.; Kannan, D. 2019. Interactive Color Image Segmentation using HSV Color Space. Interactive Color Image Segmentation using HSV Color Space. Science & Technology Journal 7(1): 37-41. DOI: 10.22232/stj.2019.07.01.05

Hirt, C. 2018. Artefact detection in global digital elevation models (DEMs): the Maximum Slope Approach and its application for complete screening of the SRTM v4.1 and MERIT DEMs. Remote Sens. Environ. 207, 27–41. https://doi.org/10.1016/ j.rse.2017.12.037

Karátson, D.; Yepes, J.; Favalli, M.; Rodríguez-Peces, M.J.; Fornaciai, A.; 2016. Reconstructing eroded paleovolcanoes on Gran Canaria, Canary Islands, using advanced geomorphometry. Geomorphology 253, 123–134

Kastner, S.; Enters, D.; Ohlendorf, C.; Haberzettl, T.; Kuhn, G.; Lücke, A.; Mayr, C.; Reyss, J.L.; Wastegård, S.; Zolitschka, B. 2010. Reconstructing 2000 years of hydrological variation derived from laminated proglacial sediments of Lago del Desierto at the eastern margin of the Southern Patagonian Ice Field, Argentina. Global Planet Change 72: 201–214

Kereszturi, G.; Németh, K.; Moufti, M.R.; Cappello, A.; Murcia, H.; Ganci, G.; Del Negro, C.; Procter, J.; Zahran, H.M.A. 2016. Emplacement conditions of the 1256AD Al-Madinah lava flow field in Harrat Rahat, Kingdom of Saudi Arabia-Insights from surface morphology and lava flow simulations. J. Volcanol. Geotherm. Res. 309, 14–30.

Kervyn, M.; Goossens, G.; Jacobs, P.; Ernst, G.G.J. 2006. Mapping volcano topography with remote sensing: ASTER vs SRTM. Int. J. Remote Sens. X (X). https://doi.org/ 10.1080/01431160802167949.

Kilian, R. 1990. The Australandean Volcanic Zone (South Patagonia). In: Symposium international ‘‘Geodynamique andine’’: Résumés des communication: 301–304. Grenoble, France.

Kobayashi, C.; Orihashi, Y.; Hiarata, D.; Naranjo, J.A.; Kobayashi, M.; Anma, R. 2010. Compositional variations revealed by ASTER image analysis of the Viedma Volcano, southern Andes Volcanic Zone. Andean Geology 37 (2): 433-441

Kölliker, A.; Kühn, F.; Reichert, F.; Tomsen, A.; Witte, L. 1917. Patagonia. Resultado de las expediciones realizadas en 1910 a 1916. Sociedad Científica Alemana Tomo II. Buenos Aires.

Lista, R. 1880. Mis Esploraciones y Descubrimientos en la Patagonia 1877 – 1880. Imprenta de Martin Biedma: 213 p. Buenos Aires.

Lliboutry, L. 1956. Nieves y Glaciares de Chile. Fundamentos de Glaciología. Universidad de Chile: 471 p. Santiago

Lliboutry, L. 1957. Banding and volcanic ash on Patagonian glaciers. Journal of Glaciology 3(21): 18-25.

Lliboutry, L. 1998. Glaciers of the Wet Andes. In: Glaciers of South America (Williams, J.; Ferringo, R. Editors). US Geological Survey Professional Paper 1386-I: 148–206

Martinic, M. 1960a. El misterioso volcán de la Patagonia. In: La Prensa Austral*,* 7th January, Punta Arenas.

Martinic, M. l960b. Descubrimiento de un nuevo volcán en la Patagonia. Revista Geográfica de Chile Terra Australis 18: 188-192.

Martinic, M. 1982. Hielo Patagónico Sur. Publicaciones del Instituto de la Patagonia. Punta Arenas.

Martinic, M. 1988. Actividad volcánica histórica en la región de Magallanes. Rev Geol Chile 15:181–186

Martinic, M. 2008. Registro histórico de antecedentes volcánicos y sísmicos en la Patagonia Austral y la Tierra del Fuego. Magallania 36: 5–18

Martinic, M. 2016. La erupción del Volcán de los Gigantes (Lautaro) en 1883. Algunas Consideraciones. Magallania 44: 65–6

Martin, C. 1909. Landeskunde von Chile. Verlag von L. Friedererichsen & Co.: 778 p. Hamburg.

Mashimbye, Z.E.; Petrus de Clercq, W.; Van Niekerk, A.. 2014. An evaluation of digital elevation models (DEMs) for delineating land components. Geoderma 213, 312–319. https://doi.org/10.1016/j.geoderma.2013.08.023.

Mayr, C.; Smith, R.E.; Luján García, M.; Massaferro, J.; Lucke, A.; Dubois, N.; Maidana, N.I.; Meier, W.J.H.; Wissel, H.; Zolitschka, B. 2019. Historical eruptions of Lautaro Volcano and their impacts on lacustrine ecosystems in southern Argentina. J Paleolimnol 62: 205–221. https://doi.org/10.1007/s10933-019-00088-y

Millan, R.; Rignot, E.; Rivera, A.; Martineau, V.; Mouginot, J.; Zamora, R.; Uribe, J.; Lenzano, G.; de Fleurian, B.; Li, X.; Gim, Y.; Kirchner, D. 2019. Ice thickness and bed elevation of the Northern and Southern Patagonian Icefields. Geophysical Research Letters, 46: 6626–6635. https://doi.org/10.1029/2019GL082485

Minowa, M.; Schaefer, M.; Skavarca, P.; Matoba, S.; Gacitua, G. 2019. Glaciological traverse across the Southern Patagonia Icefield. Bulletin of Glaciological Research 37: 47-56. Doi: 10.5331/bgr.19R03

Moreno, F.P. 1879. Viaje a la Patagonia Austral Emprendido bajo los auspicios del Gobierno Nacional 1876-1877. Tomo Primero. Imprenta de la Nacion 2nd Ed.: 462 p. Buenos Aires, Argentina

Moreno, H.; Lara, L.E.; Orozco, G. 2010. Geología del volcán Osorno, escale 1:50.000, Región de Los Lagos. Servicio Nacional de Geología y Minería, Carta Geológica de Chile, Serie Geología Básica 126: 31 p. Santiago.

Motoki, A.; Orihashi, Y.; Naranjo, J.A.; Hirata, D.; Hosono, T.; Cario, F.D.; Anma, R. 2003. Geologic occurrence and recent eruptive materials of the Lautaro Volcano, Chilean Patagonia. Journal of the Geological Society of Japan 109-5: IX-X.

Motoki, A.; Orihashi, Y.; Naranjo, J.; Hirata, D.; Skvarca, P.; Anma, R. 2006. Geologic reconnaissance of Lautaro Volcano, Chilean Patagonia. Rev Geol Chile 33: 177–187

Moyano, C.M. 1931. Viajes de exploración a la Patagonia: 1877-1890. Mercatali. Buenos Aires.

Nakamura, K. 1977. Volcanoes as possible indicators of tectonic stress orientation-principle and proposal. J. Vol. Geotherm. Res. 2: 1-16

Orihashi, Y.; Naranjo, J.A.; Motoki, A.; Sumino, H.; Hirata, D.; Anma, R.; Nagao, K. 2004. The Quaternary volcanic activities of Hudson and Lautaro volcanoes, Chilean Patagonia: new constraints from K-Ar ages. Revista Geológica de Chile 31 (2): 207-224.

Parrot, J.F.; Ramírez Núñez, C.. 2016. LiDAR DTM: artifacts, and correction for river altitudes. Investigaciones Geogr´aficas, Boletín del Instituto de Geografía 90, 28–39. https://doi.org/10.14350/rig.47372

Petit-Breuilh, M.E. 2022. La historia eruptiva de los volcanes hispanoamericanos (Siglos XVI al XX): El modelo Chileno. Trébol Ediciones: 365 p. Valparaiso, Chile

Principe, C.; Lavorini, G.; Vezzoli, L. 2017. Il Vulcano di Monte Amiata. Curatori volume collettaneo, Edizioni Scientifiche e Artistiche: 399 p. Nola. ISBN ISBN 978-88-99742-32-4

Puig, A.; Herve, M.; Suárez, M.; Saunders, A.D. 1984. Calc-alkaline and alkaline Miocene and calc-alkaline recent volcanism in the Southernmost Patagonian Cordillera, Chile. Journal of Volcanology and Geothermal Research 21 (1–2): 149-163

Quensel, P.D. 1910. Geologisch-petrographische Studien in der Patagonischen Cordillera. Bull of Geol. Upsala, Mineralog. Geol. Inst. d. Universität

Ramos, V.; Niemeyer, H.; Skarmeta, J.; Muñoz, J. 1982. Magmatic Evolution of the Austral Patagonian Andes. Earth-Science Reviews 18: 411-443

Reichert, F. 1947. Auf Berges und Lebenshöhe. Kave 2: 650 p. Buenos Aires.

Rivera, A. 2018. Glaciar Pío XI: La excepción a la tendencia de desglaciación en Patagonia. Revista Geográfica de Chile Terra Australis 54: 1–12

Sakakibara, D.; Sugiyama, S. 2014. Ice-front variations and speed changes of calving glaciers in the Southern Patagonia Icefield from 1984 to 2011. J. Geophys. Res. Earth Surf. 119: 2541–2554. doi:10.1002/2014JF003148.

Sapper, K. 1917. Katalog der Geschichtlichen Vulkanausbrüche. Karl J. Trübner, Strasburg.

Sellés, D.; Moreno, H. 2011. Geología del volcán Calbuco, escale 1:50.000, Región de Los Lagos. Servicio Nacional de Geología y Minería, Carta Geológica de Chile, Serie Geología Básica 130: 38 p. Santiago.

Sepúlveda, J.P.; Cioni, R.; Aravena, A. 2023. Morphology-based characterization of intermediate to silicic lava flows: Application to the Central Andean Volcanic Zone. Earth-Science Reviews 241, 104433. https://doi.org/10.1016/j.earscirev.2023.104433

Sepúlveda, J.P.; Cioni, R.; Alni, E.; Scaillet, S.; Ureta, G.; Aguilera, F.; Scaillet, B. 2025. Emplacement dynamics of the debris avalanche deposits from the Ollagüe Volcano, Central Volcanic Zone of the Andes. Landslides. DOI 10.1007/s10346-025-02565-0

Sepúlveda, J.P.; Paternostro, S., Valeriani, L.; Masetti, G.; Aravena, A.; Lo Faro, S.; Vita, L.; Conticelli, S.; Cioni, R. 2026. Application of Red Relief Image Maps as a complementary tool for mapping volcanic areas: The case of the Monte Amiata volcano, Italy. Geomorphology, 499, 110195.

Shipton, E. 1960. Volcanic activity of Patagonian Ice Cap. Geographical Journal 126: 389 p

Shipton, E. 1963. Land of Tempest: Travels in Patagonia 1958-62. The Travel Book Club. London.

Smith, R.; Smith, V.C.; Fontijn, K.; Gebhardt, A.K.; Wastegård, S.; Zolitschka, B.; Ohlendorf, C.; Stern, C.; Mayr, C. 2019. Refining the Late Quaternary tephrochronology for southern South America using the Laguna Potrok Aike sedimentary record. Quaternary Science Reviews 218: 137-155.

Stern, C.R.; Skewes, A.; Durán, M. 1976. Volcanismo Orogénico en Chile Austral. In: Primer Congreso Geológico Chileno, 2-7 August, Santiago, Chile.

Stern, C.R.; Futa, K.; Muehlenbachs, K. 1984. Isotope and trace element data for orogenic andesites from the Austral Andes. In: Andean magmatism: chemical and isotopic constraints (Harmon, R.S.; Barreiro, B.A. Editors) Shiva Publishing:31–46. Cheshire.

Stern, C.R.; Kilian, R. 1996. Role of the subducted slab, mantle wedge and continental crust in the generation of adakites from the Andean Austral Volcanic Zone. Contrib Mineral Petrol 123: 263–281.

Stern, C. 2004. Active Andean volcanism: its geologic and tectonic setting. Revista Geológica de Chile 31(2): 161-206.

Stern, C. 2007. Holocene tephrochronology record of large explosive eruptions in the southernmost Patagonian Andes. Bull Volcanol 70: 435–454. Doi.10.1007/s00445-007-0148-z

Stern, C.R.; Moreno, H.; López-Escobar, L.; Clavero, J.; Lara, L.E.; Naranjo, J.A.; Parada, M.A.; Skewes, M.A. 2007. Chilean Volcanoes. In: The Geology of Chile (Moreno, T.; Gibbons, W. Editors) The Geological Society: 414p. London.

Suárez, J.; Ghiglione, M.C.; Calderón, M.; Sue, C.; Martinod, J.; Guillaume, B.; Rojo, D. 2019. The metamorphic rocks of the Nunatak Viedma in the Southern Patagonian Andes: Provenance sources and implications for the early Mesozoic Patagonia-Antarctic Peninsula connection. Journal of South American Earth Sciences 90: 471–486

The South American Missionary Magazine. 1880. The South American Missionary Society XV: 286 p. London.

Ulusoy, I.; Diker, C.; Şen, E.; Aydın, E.; Akkaş, E.; Gümüş, E.; Çubukçu, H.E.; Erkut. V. 2021. Surface expressions of morphostructural features at Hasandağ stratovolcano on DEM datasets. Mediterranean Geoscience Reviews 3: 175-191. doi.org/10.1007/s42990-020-00044-3

Van Wees, R.M.J.; O´Hara, D.; Kereszturi, G.; Grosse, P.; Lahitte, P.; Tournigand, P.Y., Kervyn, M. 2024. Towards more consistent volcano morphometry datasets: Assessing boundary delineation and DEM impact on geometric and drainage parameters. Geomorphology 465, 109381. https://doi.org/10.1016/j.geomorph.2024.109381

Vezzoli, L.; Tibaldi, A.; Renzulli, A.; Menna, M.; Flude, S. 2008. Faulting-assisted lateral collapses and influence on shallow magma feeding system at Ollagüe volcano (Central Volcanic Zone, Chile-Bolivia Andes). Journal of Volcanology and Geothermal Research 171(1–2): 137-159

Villegas, D.; Pereyra, F.; Viaggio, A.; Ferrer, J. 2009. Ocurrencia de materiales piroclásticos en suelos de tres sectores del oeste de Santa Cruz. Revista de la Asociación Geológica Argentina 64(2): 303 - 311

von Rentzell, I. 1933. La expedición Argentina a la región de los hielos patagónicos al Oeste del lago San Martín. In: La Prensa, 2, pag. 3, 10th December, Buenos Aires,

von Rentzell, I. 1934a. La expedición Argentina a la región Oeste del lago San Martín. In: La Prensa, 2, pag. 3, 21th January, Buenos Aires.

von Rentzell, I. 1934b. La expedición Argentina a la región inexplorada del Oeste del lago San Martín. Travesía por los hielos del interior. In: La Prensa, 2, pag. 4, 25th March, Buenos Aires.

von Rentzell, I. 1934c. La expedición Argentina los hielos interiores de la Patagonia. Mi última aventura entre ellos. In: La Prensa, 2, pag. 4, 21th July, Buenos Aires.

Warren, C.R.; Sugden, D.E. 1993. The Patagonian icefields: A glaciological review. Arct. Alp. Res. 25(4): 316–331.

Warren, C.; Rivera, A.; Post, A. 1997. Greatest Holocene advance of Glaciar Pio XI, Chilean Patagonia: Possible causes. Annals of Glaciology 24: 11-15.

Wastegård, S.; Veres, V.; Kliem, P.; Hahn, A.; Ohlendorf, C.; Zolitschka, B.; The PASADO Science Team. 2013. Towards a late Quaternary tephrochronological framework for the southernmost part of South America e the Laguna Potrok Aike tephra record. Quaternary Science Reviews, 71, 81-90. http://dx.doi.org/10.1016/j.quascirev.2012.10.019

Wilson, R.; Carrión, D.; Rivera, A. 2016. Detailed dynamic, geometric and supraglacial moraine data for Glaciar Pio XI, the only surge-type glacier of the Southern Patagonia Icefield. Annals of Glaciology 57 (73): 119 – 130. DOI: https://doi.org/10.1017/aog.2016.32

Yokoyama, R.; Shirasawa, M.; Pike, R.J. 2002. Visualizing Topography by Openness: A New Application of Image Processing to Digital Elevation Models. Photogrammetric Engineering & Remote Sensing 68(3): 257-265.

Yokoyama, I. 2015. Eruption patterns of parasitic volcanoes. Annals of Geophysics 58 (3) S0327. 10.4401/ag-6557

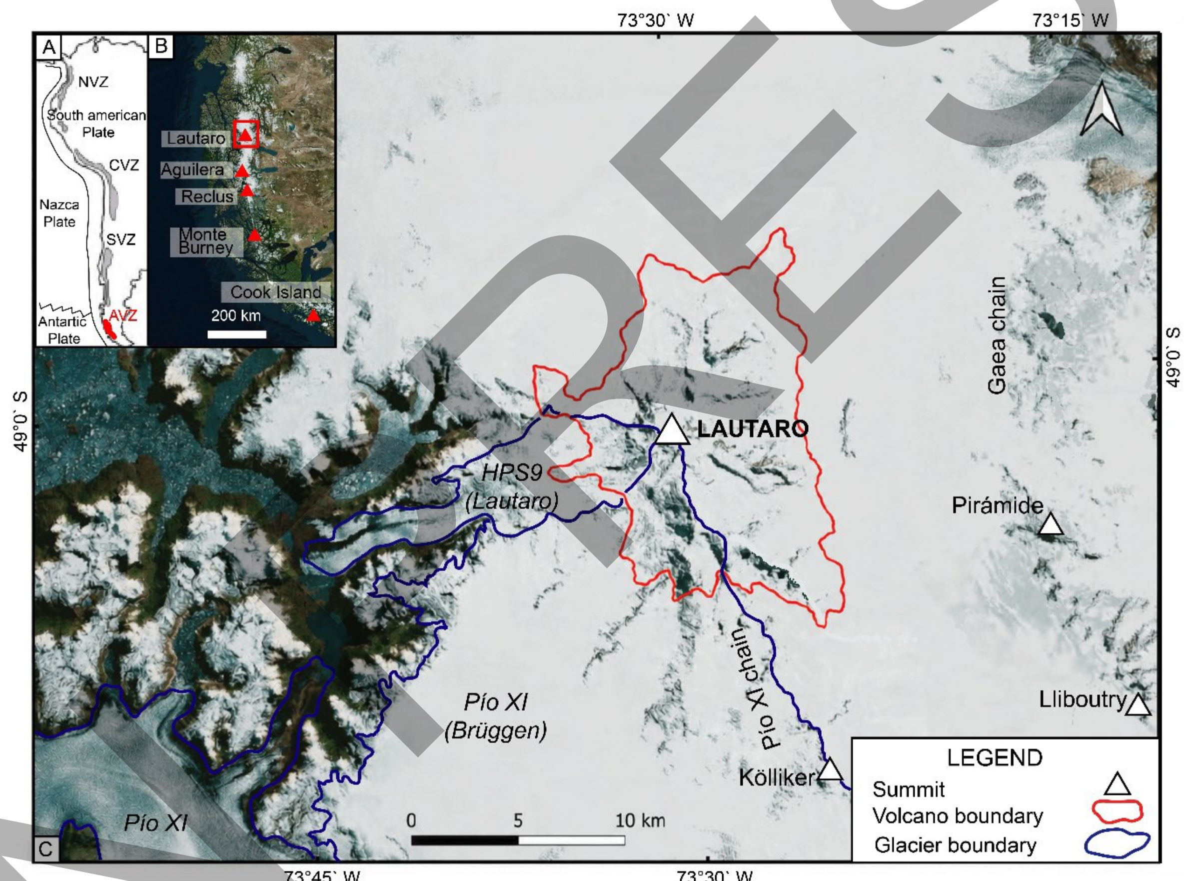

Fig. 1. A. Location map of the Austral Volcanic Zone (AVZ) of the Andes. NVZ: Northern Volcanic Zone, CVZ: Central Volcanic Zone, SVZ: Southern Volcanic Zone. **B.** Location of the Lautaro volcano within the Southern Patagonian Ice Field. **C.** Satellite image from the Bing Map repository showing the Lautaro volcano covered by a permanent ice blanket. The boundaries of the glaciers are simplified from the Inventario Nacional de Glaciares from the Dirección General de Aguas, Ministerio de Obras Públicas, Chile. S/n = No name. Volcano boundary obtained after Red Relief Image Map (RRIM) processing (see text for details).

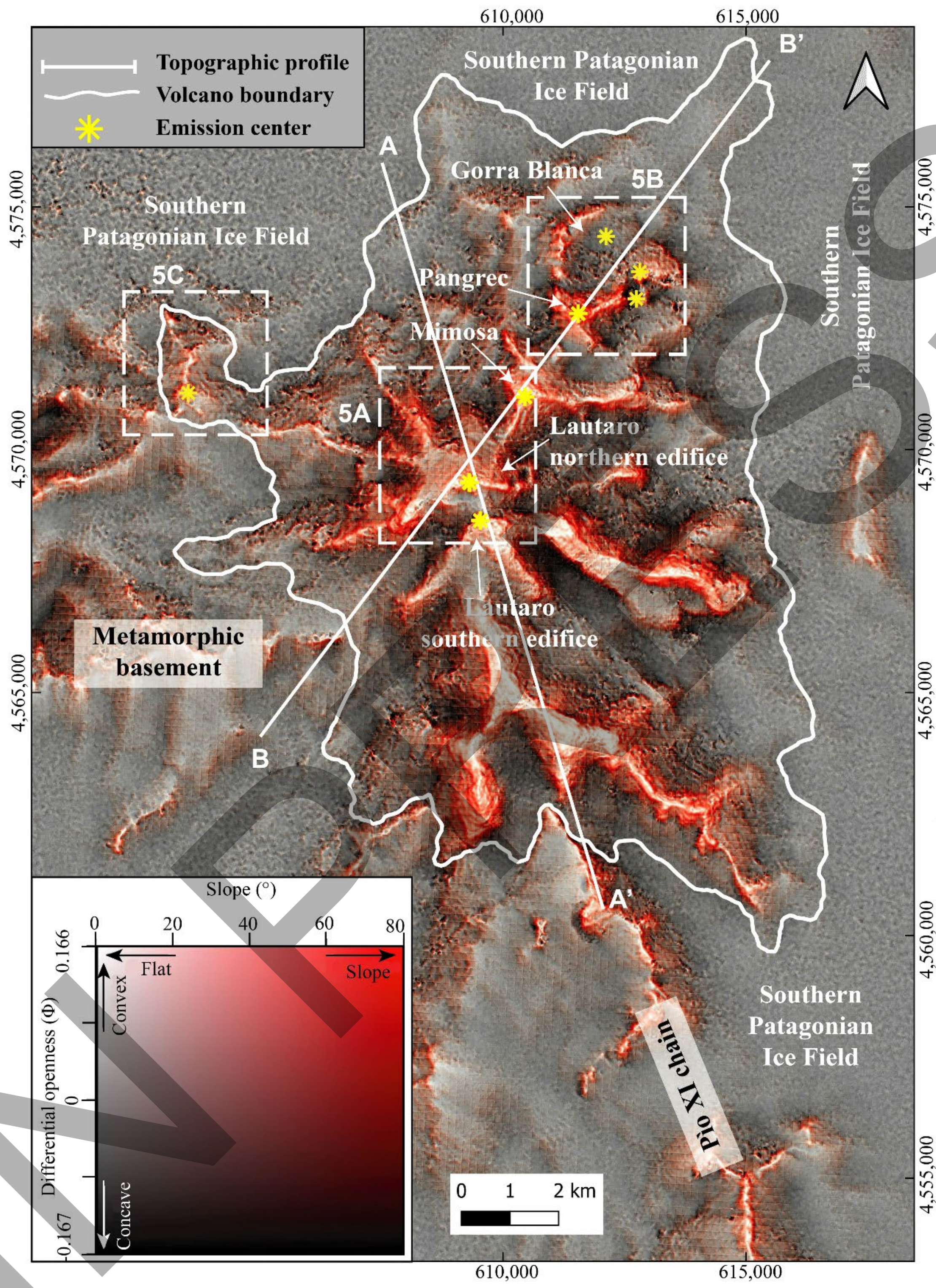

Fig. 2. Red Relief Image Map (RRIM) showing the Lautaro volcano and the northern part of the Pío XI chain. RRIM generated by applying a 1,000 m search radius. Positive relief landforms are displayed as white, bottom valleys as black, steep slopes as bright red, and flat surfaces as grey. White dotted boxes refer to enlarged areas in figures 5 and 8.

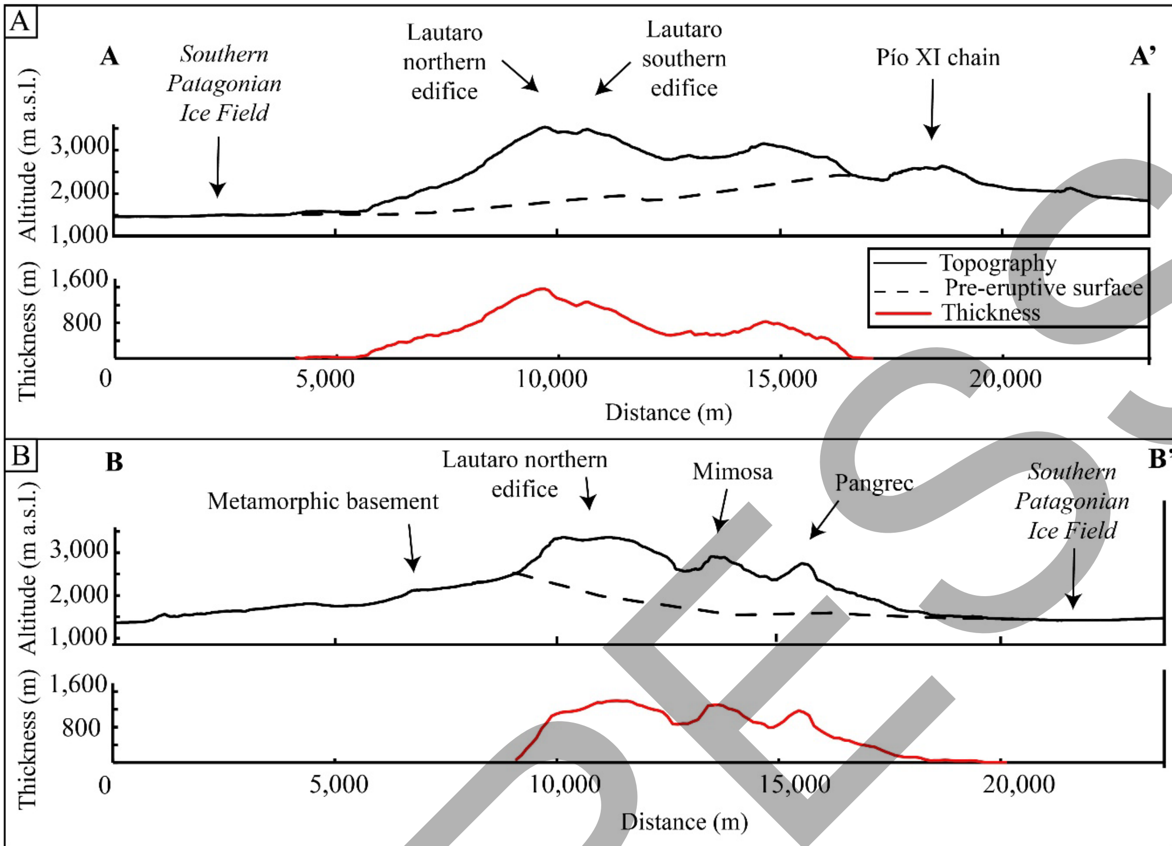

Fig. 3. Topographic, pre-eruptive, and thickness profiles along two transects crossing Lautaro volcano. **A.** AA' transect (NW-SE oriented). **B.** BB' transect (SW-NE oriented). See figure 2 for transect locations. See text for pre-eruptive surface acquisition.

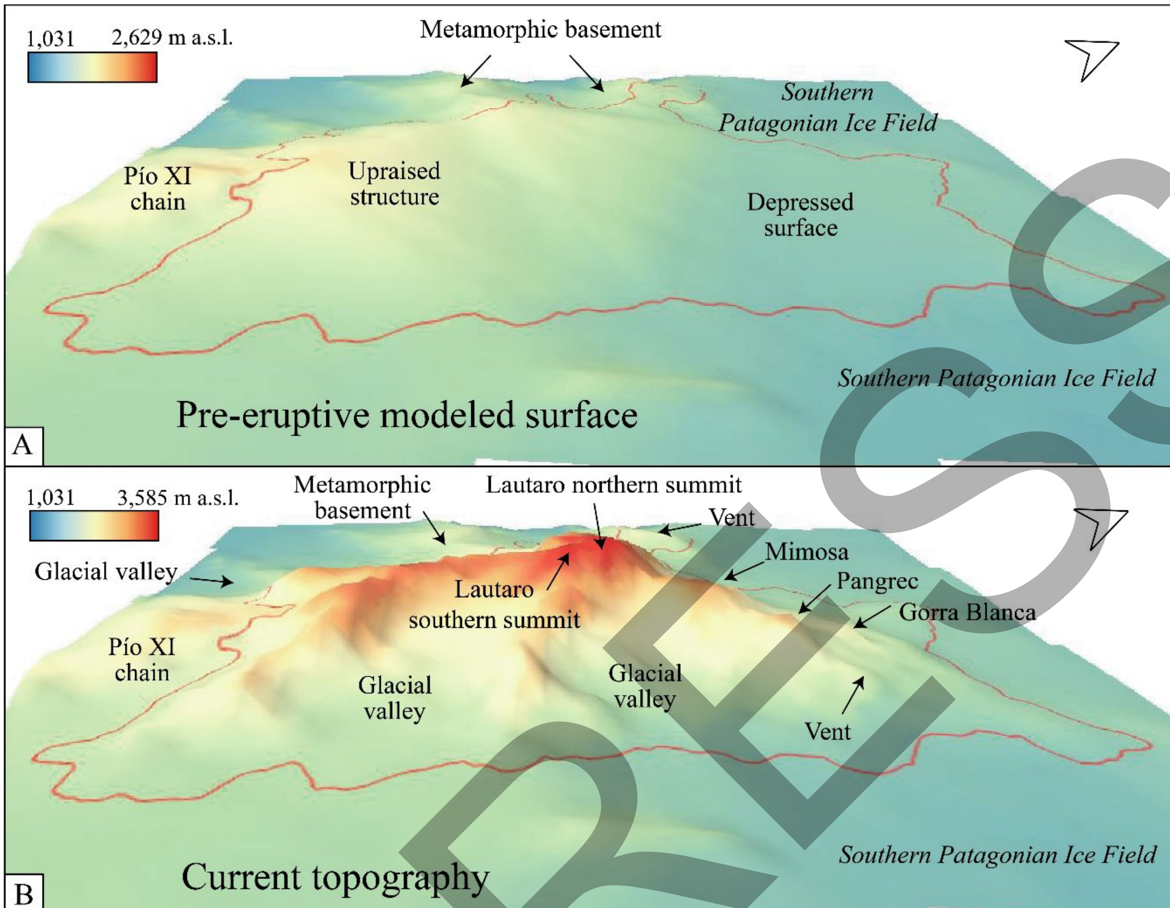

Fig. 4. A. Pre-eruptive surface from the Lautaro volcano area, showing a depressed surface towards the northeastern sector and an upraised structure towards the southwest, the latter possibly part of the Pío XI chain. **B.** Current topography. See text for pre-eruptive surface acquisition. Vertical exaggeration: 1.2. View to the west.

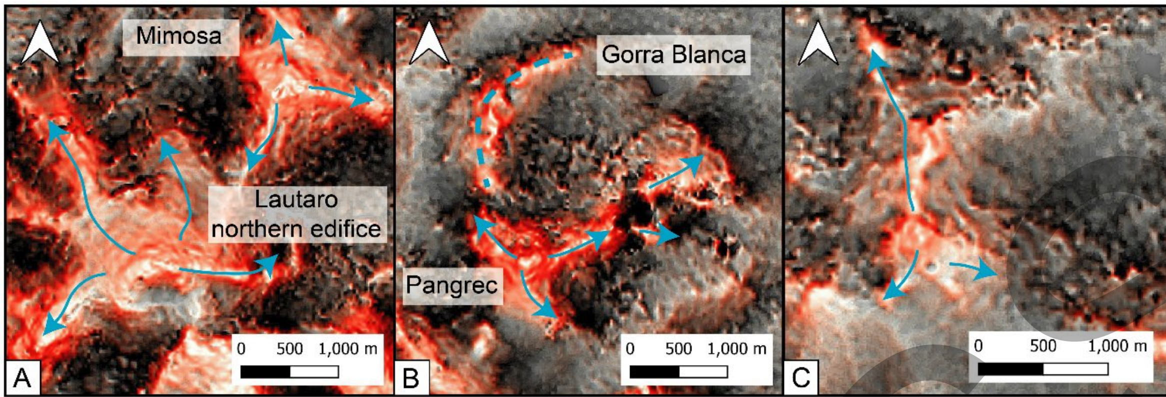

Fig. 5. RRIM-derived excerpts from figure 2, obtained by applying a 1,000 m search radius. **A.** Northern edifice and Mimosa emission center, formed by overlapped, radial lavas. One lava flow from the northern edifice was diverted by Mimosa, indicating an older age for the latter. **B.** NE flank of Lautaro, with Pangrec lavas cutting the ancient Gorra Blanca caldera structure. **C.** Parasitic center at the WNW flank of Lautaro, with a lava flow emplaced towards its northern flank. Blue arrows indicate lava flow emplacement directions.

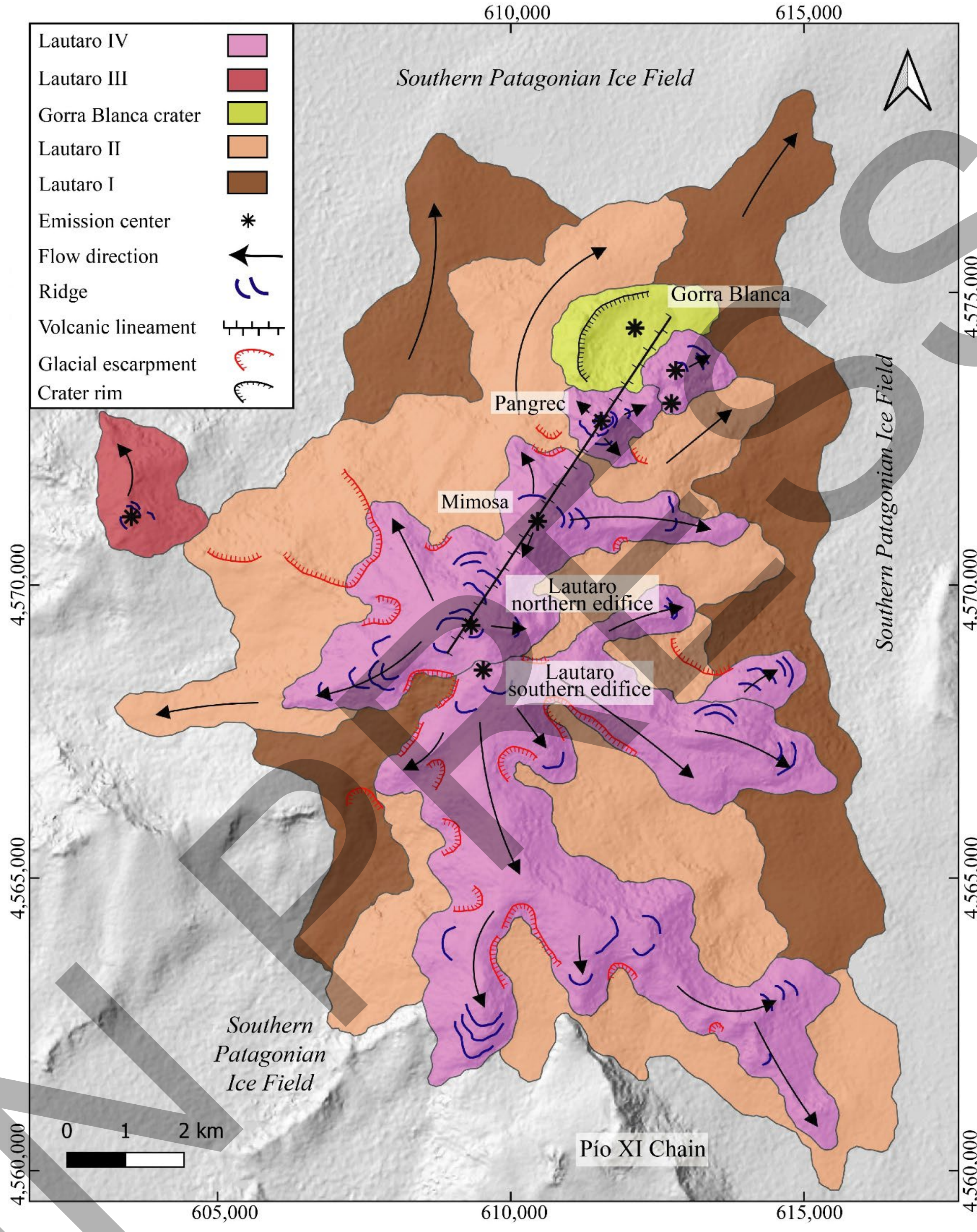

Fig. 6. ALOS PALSAR-derived shaded relief image showing the geomorphological units identified from the RRIM for the Lautaro volcano. See text for explanations.

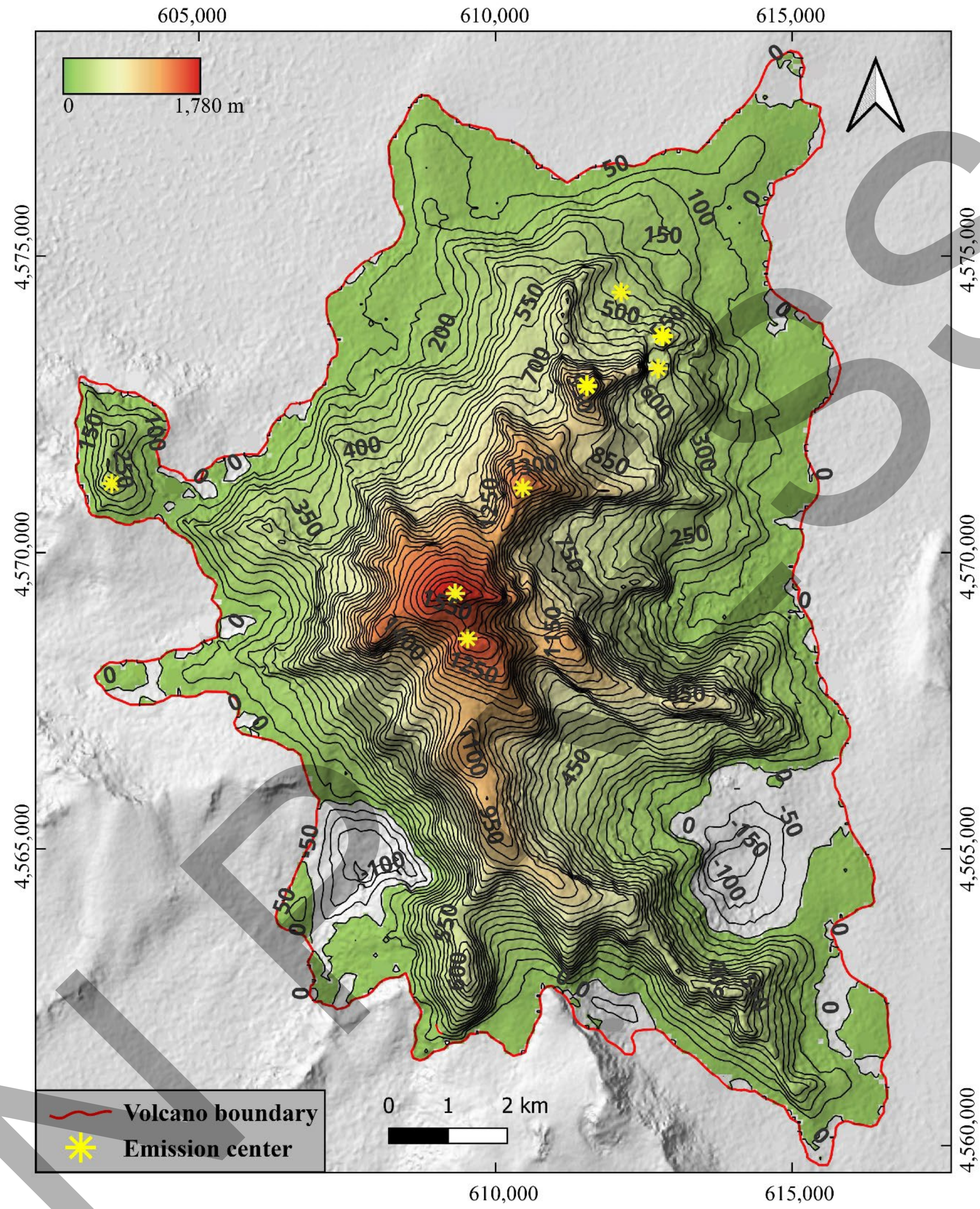

Fig. 7. Isopach map for the Lautaro volcano with isocurves every 50 m. Negative thicknesses occur where interpolation underestimates true pre-eruption topography due to the edge effect or erosional valleys. Maximum thicknesses for the volcano occur within the depressed surface along the northern summit and the NE-SW lineament.

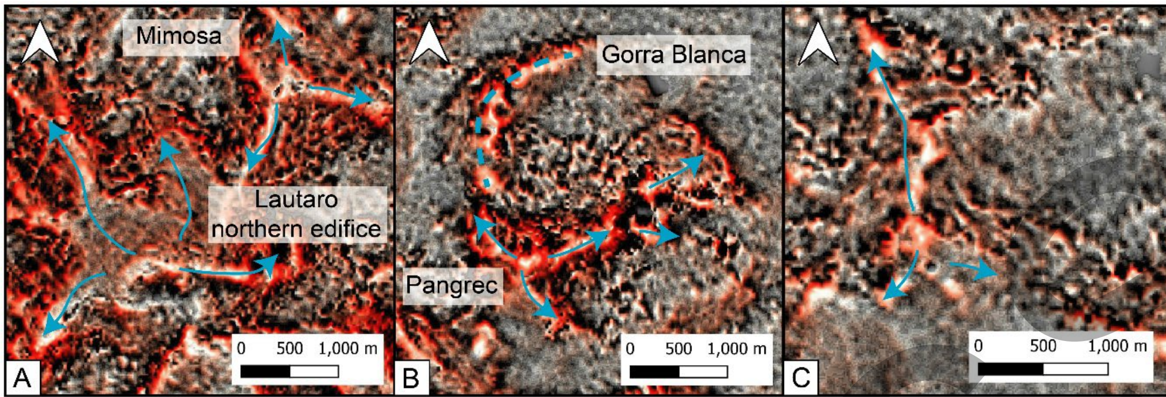

Fig. 8. RRIM-derived panels from figure 5, obtained by applying a 100 m search radius (instead of a 1,000 search radius, as in figure 5). Blue arrows indicate lava flow emplacement directions. **A.** Northern edifice and Mimosa emission center, showing background noise with no identifiable small lava lobes. **B.** Pangrec and Gorra Blanca centers showing flat surfaces and hardly identifiable lava flows. **C.** Parasitic center at the WNW flank of Lautaro, showing large background noise and major presence of unfilled voids artifacts, limiting the tracing of the lava flow boundary.

Table 1. Record of historical activity of the Lautaro volcano

* Previously assigned to the Viedma nunatak (then a potential volcano)

- No reported data

Year of eruption	Place of observation	Type of activity	Observation	Reference
1712	-	-	No available description or bibliographic source	Petit-Breuilh (2022)
1824	-	-	No available description or bibliographic source	Petit-Breuilh (2022)
September 17th, 1864	-	>1,000 m eruptive column	No available bibliographic source	Petit-Breuilh (2022)
October 12th, 1876	Messier Channel, 70 km W of Lautaro	Ash fallout	Ash fallout on the desk of the Brigantine Sunbeam	Brassey (1881)
1877	-	-	Eruption reported south of Middle Island, 90 km NW of Lautaro	Göll (1904)
December 12th, 1877	Lake Argentina, 150 km SE of Lautaro	Rumbles (explosions)	Thomas Rogers mentioned Chaltén or Fitz Roy as a possible source	Kölliker et al. (1917)
1878	Lake Viedma, SE of Lautaro	Steam column	Assigned to Fitz Roy. Gas and ash emissions observed during this period by aónikenk local population	Lista (1880)
1878	Omaha gunboat, W of Lautaro	Ash fallout	-	Lista (1880)
August 8th, 1879	H.M.S. Gannet, Puerto Gray, 60 km NW of Lautaro	1,500-1,800 m eruptive column	Eruptions repeated at intervals of three hours. First graphic record of an eruption from Lautaro, with an engraving published in the South American Missionary	The South American Missionary Magazine (1880), Martinic (2008)

			Magazine (1880), entitled "Volcano in Smyth's Sound, Straits of Magellan viewed from H.M.S. Gannet".	
1879	Someplace between San Martin and Viedma lakes	Ash/tephra column (?)	-	Martin (1909), Sapper (1917)
1883	Upper basin of Coyle River, 250 km SE of Lautaro, Argentina	Ash fallout, explosions, eruptive column, incandescence	Mentioned as *Volcán de los Gigantes*. Incandescence with explosions lasting for minutes during the first night followed by a dense black, umbrella-like tephra column with pulsating activity and ashfall of up to 5 cm thick. Activity may lasted for seven days.	Greenwood (2015), Martinic (2016)
1884	Lake Viedma, SE of Lautaro	Ash fallout, explosions, eruptive column, incandescence	Dense and pulsating eruptive column from the Chaltén volcano (i.e., Lautaro) with ashfall and underground noises. Incandescence observed during the night	Kölliker et al. (1917)
May, 1886	Valley of Santa Cruz, 200 km SE of Lautaro	Ash fallout	Fallout in Punta Arenas, covering vast expanses of grasslands. Waters of the Santa Cruz River suddenly rose (possibly glacial outburst flood). Lautaro or Aguilera as possible sources	Burmeister (1891)
1910	-	Eruptive column	-	Petit-Breuilh (2022)
1933	Base of Lautaro volcano	Ash emission	First expedition to Lautaro by Federico Reichert, Ilse von Rentzell, Juan Neumayer, and Arturo Donat. Not widely disseminated	von Rentzell (1933, 1934a,b,c), Reichert (1947)
1935	SPI northwest of Fitz Roy	Glaciar melting and tephra blanket	Assigned to a nearby unknown volcano	de Agostini (1945)
1945	Trimetrogon Aerial Photographic Surveys	Glaciar melting and tephra blanket	Identified in February 1946 and assigned to a possible eruption of Lautaro	Lliboutry (1956)
February, 1952 *	Trimetrogon Aerial Photographic Surveys	Tephra blanket	Assigned to Viedma volcano (now a nunatak)	Lliboutry (1956)
December 28th, 1959	Overflight	Tephra column	First overflight by Alfonso Cuadrado Merino, a pilot from the *Linea Aérea Nacional*	Martinic (1960a)
January 19th, 1960	Base of Lautaro volcano	Ash amission and tephra column	Excursion composed of Eric Shipton, Jack Ewer, Cedomir Marangunic, and Eduardo García. Location established cartographically	Shipton (1960)
October 2th, 1961	Overflight	Gas and ash emission	Reported by the Press Office of the Chilean Air Force	Casertano (1962)
1972	Argentina	-	Oral communication from settlers	Lliboutry (1998)
June, 1978	Argentina	-	Oral communication from settlers	Lliboutry (1998)

1979	Landsat 3 RBV image	Tephra blanket	Image from 8th March. Tephra at distances of up to 110 km south of Lautaro	Lliboutry (1998)
September-November 1988*	Viedma Glacier	Glacier melting and tephra blanket	Assigned to Viedma volcano (now a nunatak)	Kilian (1990)
1995	-	-	No available cited bibliography or records of volcanic activity	Petit-Breuilh (2022)
1998	-	-	No available cited bibliography or records of volcanic activity	Petit-Breuilh (2022)